Evaluation and improvement of empirical models of global solar irradiation: case study northern Spain

F. Antonanzas-Torres[a,*], A. Sanz-Garcia[a], F. J. Martínez-de-Pisón-Ascacíbar[a], O. Perpiñán-Lamigueiro[b,c]

[a]EDMANS Group, Department of Mechanical Engineering, University of La Rioja, Logroño, Spain.
[b]Electrical Engineering Department, EUITI-UPM, Ronda de Valencia 3, 28012 Madrid, Spain.
[c]Instituto de Energía Solar, Ciudad Universitaria s/n, Madrid, Spain

---

Abstract

This paper presents a new methodology to build parametric models to estimate global solar irradiation adjusted to specific on-site characteristics based on the evaluation of variable importance. Thus, those variables higly correlated to solar irradiation on a site are implemented in the model and therefore, different models might be proposed under different climates. This methodology is applied in a study case in La Rioja region (northern Spain). A new model is proposed and evaluated on stability and accuracy against a review of twenty-two already existing parametric models based on temperatures and rainfall in seventeen meteorological stations in La Rioja. The methodology of model evaluation is based on bootstrapping, which leads to achieve a high level of confidence in model calibration and validation from short time series (in this case five years, from 2007 to 2011).

The model proposed improves the estimates of the other twenty-two models with average mean absolute error (MAE) of 2.195 MJ/m^{2}day and average confidence interval width (95% C.I., n=100) of 0.261 MJ/m^{2}day. 41.65% of the daily residuals in the case of SIAR and 20.12% in that of SOS Rioja fall within the uncertainty tolerance of the pyranometers of the two networks (10% and 5%, respectively). Relative differences between measured and estimated irradiation on an annual cumulative basis are below 4.82%. Thus, the proposed model might be useful to estimate annual sums of global solar irradiation, reaching insignificant differences between measurements from pyranometers.

Keywords: Solar global irradiation, empirical models, time series, evapotranspiration

---

Nomenclature

BC Bristow & Campbell model

ΔT Daily range of maximum and minimum temperatures

$\overline{\Delta T_c}$ Average ΔT of the *calibration* dataset

ΔT_{i-1} Daily range of maximum and minimum temperatures on day *i-1*

ΔT_m Monthly average of ΔT

$\overline{\Delta T_t}$ Average ΔT of the *testing* dataset

h Elevation above sea level

*Corresponding author
Email address: `antonanzas.fernando@gmail.com` (F. Antonanzas-Torres)

Preprint submitted to Renewable Energy *May 14, 2013*

H Daily mean relative humidity

J Julian day

M Logical variable of rainfall

MAE_{tes} Mean absolute error of testing

MAE_{val} Mean absolute error of validation

$\overline{MAE_{val}}$ Average MAE_{val} for the whole set of stations

n Length in days of the *validation* database

P Rainfall

P_c Yearly average rainfall in mm for the *calibration* dataset

P_t Yearly rainfall in mm for the *testing* dataset

$p_{sat}\left[T_{max}\right]$ Vapor saturation pressure at T_{max}

R^2 Coefficient of determination

R_a Extraterrestrial irradiation

$R_{a,i-30}$ Extraterrestrial irradiation on day *i-30*

R_s Daily global solar irradiation

$\overline{R_s}$ Monthly mean of daily global irradiation

$\overline{R_{s,c}}$ Average R_s for the *calibration* period

$R_{s,est}$ Daily estimated irradiation

$R_{s,meas}$ Daily measured irradiation

$\overline{R_{s,t}}$ Average R_s for the *testing* period

$\overline{R_{MAE,val}}$ Average confidence interval width of MAE

$\overline{R_{RMSE,val}}$ Average confidence interval width of RMSE

$\overline{RMSE_{val}}$ Average $RMSE_{val}$ for the whole set of stations

$RMSE_{tes}$ Root mean square error of testing

T_{avg} Daily average air temperature

T_{max} Daily maximum temperature

T_{min} Daily minimum temperature

θ Julian angle

W Daily mean wind speed

1. Introduction

Solar irradiation research is a field of rising interest due to its many applications, such as the study of evapotranspiration [1] and optimization of water demand in irrigation, crop forecasting [2] from near-to-present measurements and estimates, the development and reduction of uncertainties in solar energy technologies (generation and internal rate of return) [3], the adjustment of energy policies to promote solar energies, and research on climate change [4]. The high cost of measuring solar irradiation with pyranometers and the scarcity of long, reliable datasets for specific locations has propitiated the progress in estimators such as the analysis of satellite images [4, 5], artificial neural networks (ANN) [6, 7] and empirically-based parametric models [8–10]; the latter estimating daily global horizontal irradiation (R_s) from other meteorological variables.

Satellite-based R_s estimates are only provided with high resolution for specific areas in the planet, for example, 70S-70N, 70W-70E in the Satellite Application Facility for Climate Monitoring (CM SAF) [11], Helioclim1 and Helioclim3 from SODA [12]. In other areas, resolution from satellite-based estimates is low, such as in some regions of South America and South-East Asia (INPE [13] and the National Renewable Energy Laboratory (NREL) [14] with 40x40km resolution). The NASA Surface meteorology and Solar Energy (SSE) [15] coverage is global but resolution is very low (1x1°). Due to the effect of local microclimatic events on R_s, daily and annual divergence within a 40x40km or 1°x1° cell might be significant [16]. In addition, satellite-based daily estimates are not generally freely accesible in the near present. For instance, the SODA provides R_s from Helioclim1 for the period 1985-2005, Helioclim3 for the year 2005 and from the SSE database for the period 1983-2005. These near-to-present estimates are necessary in different applications such as the estimation of evapotranspiration of previous days to forecast irrigation. As a result, the empirically-based parametric models stand out because of their high simplicity in estimating near-to-present R_s from measurements of commonly registered variables, generally registered with a higher distribution than the satellite resolution.

[17] and [18] developed the first parametric models to estimate R_s out of sunshine records and introduced the concept of the atmospheric transmittance that affects incoming extraterrestrial irradiation (R_a). The common figure of most parametric models is that they account for latitude, solar declination, the Julian day (J), and day length by including R_a [19]. [20] included mean daily cloud coverage to explain R_s. [21] introduced relative humidity and maximum temperature to estimate the monthly mean of the daily irradiation ($\overline{R_s}$). However, the scarcity of sunshine and cloud cover records limits the usage of these methods to the location of validation.

[9], [22], and [8] developed the first models in which R_s is estimated through the daily range of maximum and minimum temperatures (ΔT). Note that in these models ΔT behaves as an indicator of atmospheric transmittance, providing information about cloud cover. The higher emissivity of clouds than clear sky makes the maximum air temperature decrease and the minimum temperature increase, and as a result the ΔT decreases [23].

[24] studied the [9] model with $\overline{R_s}$, distinguishing between inland and coastal locations and obtaining higher accuracy in monthly than in daily estimates [25]. Other authors also modified the [9] model, introducing elevation [26], or modifying the square root by a Neperian logarithm [27] (the latter attributing it to [25]).

Rainfall (P) was introduced as an explanatory variable directly [10, 28] or as a binary variable (M) equal to 1 in days with some rainfall (denoted as rainy days) and 0 in days without any rainfall recorded (non-rainy days) [29–31]. According to previous papers, [30, 31] rejected using ΔT in his model, considering P sufficient to explain R_s. [30] also rejected R_a and applied Fourier series based on the julian angle (θ), corresponding to the angle in radians of the J.

[8] (hereinafter BC) calculated ΔT as the difference between the maximum temperature of

the day and the average of the minimum temperatures of the current day and the following day. [32] modified the BC model, calculating ΔT related to rainfall. [19] studied the influence of ΔT on estimations, calculated as the difference between the maximum (T_{max}) and minimum temperatures (T_{min}) and as ΔT as per BC and evaluated it with sixteen BC and [9] derived models. Eventually, better estimations were achieved with ΔT as the difference between T_{max} and T_{min}. The BC equation has also been modified by considering some parameters as constants [1, 19, 33, 34]. The last of this papers attributed two new models to [33] and [35]. Additionally, [33] concluded that [25] and BC models perform better for $\overline{R_s}$ than for daily values. [36] and latter [35] (who referred it as BC) included the monthly mean of the daily ΔT to smooth the results of the BC model. [36] also developed a model in which the daily average temperature was introduced. [37, 38] also modified the BC model, introducing the R_a as a function of the atmospheric transmittance. Indeed, several papers have proved the efficacy of the BC model by comparing it with their own models or with other models, e.g. [1, 19, 23, 28, 29, 32–35, 39–42].

Most of parametric models to estimate R_s have been derived from the [9] and the BC models by adding other variables that were proved to achieve better estimates where validated. However, a variable which might be correlated with R_s in a site, might not have such a dependency in other site [26]. This paper proposes the evaluation of variable importance as a method to adjust general models, i.e., the BC model. New models are then built by including important variables, obtained by on-site specific relationships between predictors and R_s.

Several papers have already evaluated models according to test errors, assessing the capacity of generalization under unproven data [23, 35, 39]. Nevertheless, models might generate low test errors for a specific time series while still being unstable under slight variations in the calibration data [43]. This paper also proposes an evaluation including stability and accuracy under different initial conditions as model selection criteria, and implements it on twenty-four parametric models (including two new models built on the method of evaluation of variable importance) in seventeen meteorological stations in La Rioja (Spain). The estimates of the best performing model are also compared with the CMSAF SIS satellite-derived database.

Table 1 summarizes the twenty-four models studied.

2. Meteorological data

The assessment is performed in La Rioja, a 5028 km^2 region of Spain with significant climatic differences mainly due to differences in elevation and the smoothing influence of the Ebro River. The daily meteorological data is provided by two public agencies, SOS Rioja [44] and SIAR (Service of Agroclimatic Information of La Rioja) [45], with records taken every fifteen and thirty minutes respectively. R_s is measured by SOS Rioja with *Geonica* sensors *CM-6B* and *EQ08*, which are classed as First Class pyranometers according to the ISO9060 and by SIAR with *Kipp&Zonen CM3* and *Hukseflux LP02*, which are Second Class pyranometers with 5% and 10% daily tolerance levels respectively. The impact of the horizon effect on R_s has been analyzed and not taken into account, since sky-view factors (ratio of visible sky related to the potential visible sky) are between 0.985-0.999, substantially lower than the uncertainty of sensors and models and therefore negligible. T_{max}, T_{min} and P are recorded with tolerances of 0.1 °C and 0.1 mm by SOS Rioja and 0.2 °C and 0.2 mm by SIAR. Additionally, average wind speed (W) and relative humidity (H) are recorded with 0.3 $\frac{\mathrm{m}}{\mathrm{s}}$ and 3% tolerance respectively. Eventually, a total number of seventeen meteorological stations are selected (see Figure 1), with five complete years of daily historical data on the aforesaid variables from 2007 to 2011. Spurious data are filtered out according to the following limits, T_{max} lower than 45 °C, T_{min} higher than -20 °C, irradiance lower than 1150 $\frac{\mathrm{W}}{\mathrm{m}^2}$, R_s lower than the daily R_a, P lower than 40 $\frac{\mathrm{mm}}{\mathrm{h}}$, W lower than 30 $\frac{\mathrm{m}}{\mathrm{s}}$ and H

lower than 100%. Spurious data account for less than 0.14% and are replaced by the average of the previous and following measurements.

The time series of daily values from 2007 to 2011 of each station is divided into the *calibration* dataset, running from 2007 to 2010 and the *testing* dataset, which covers 2011 alone. Table 2 provides general information about the main variables measured during the *calibration* and *testing* periods.

Additionally, R_s from the CM SAF SIS for 2007-2011 is obtained to evaluate and compare errors from the best-performing parametric model with those from this satellite-derived database.

3. Method

3.1. Methodology of model evaluation

The analysis of robustness proposed leads to the stability of models being assessed under many different initial conditions, and it is advisable to select the most suitable model, based not only on the lowest testing errors [46]. The evaluation is based on bootstrapping to extract a large amount of knowledge from a short time series [47, 48]. It is performed with each model at each station. 80% of the *calibration* dataset for every station (1168 days) is sampled to calibrate the parameters of each model. The remaining 20% (292 days) is used to validate the calibration by calculating the validation mean absolute error (MAE_{val}) and the validation root mean square error ($RMSE_{val}$). This process is repeated one hundred times, resampling the 80% of the *calibration* dataset and calculating MAE_{val} and $RMSE_{val}$ to eventually obtain the confidence intervals of the model parameters and errors.

$$MAE_{val} = \frac{1}{n}\sum_{i=1}^{n}|(R_{s,meas} - R_{s,est})| \tag{1}$$

$$RMSE_{val} = \sqrt{\frac{1}{n}\sum_{i=1}^{n}(R_{s,meas} - R_{s,est})^2} \tag{2}$$

Where, $R_{s,meas}$ and $R_{s,est}$ stand for daily measured irradiation and daily estimated irradiation with the model to be validated. n stands for the length in days of the *validation* database (292 days).

Each model is calibrated with both spectral projected gradient methods for large-scale optimization [49] and a quasi-Newton algorithm known as the Broyden, Fletcher, Goldfarb and Shanno ($BFGS$) method [50], which updates an approximation to the inverse Hessian along with a point line search strategy [51]. The parameters calibrated minimize the sum of the square residuals between the measurements ($R_{s,meas}$) and the estimations ($R_{s,est}$). A combination of square errors in model calibration, and mean absolute errors (MAE) is chosen as indicators of model performance to reduce the impact of outliers in the evaluation [52].

The stability and accuracy of each model are assessed at the set of stations as a whole with the mean confidence interval width of MAE ($\overline{R_{MAE,val}}$) and the mean MAE ($\overline{MAE_{val}}$). The unpaired $t - test$ is also evaluated to determine if MAE_{val} means are statistically different between pairs of models within each station. The t is calculated with Equation 3 and then the $p - value$ of the null hypothesis is derived.

$$t = \frac{\overline{x_i} - \overline{x_j}}{\sqrt{\frac{s^2{}_i - s^2{}_j}{n}}} \tag{3}$$

where $\overline{x_i}$ and $\overline{x_j}$ are the mean MAE_{val} by bootstrapping with 100 samples of model i and j, s_i and s_j the standard deviations and n the number of samples.

The capacity of generalization for non-common values is assessed with the confidence interval width of RMSE ($\overline{R_{RMSE,val}}$) and the mean RMSE ($\overline{RMSE_{val}}$), as a result of the amplifying property of this statistic with outliers.

The capability for generalization under unproven continuous data [53] is assessed within the *testing* dataset with the testing MAE (MAE_{tes}). The figures for the model parameters are obtained from the median of the bootstrapping distributions.

The analysis described in this paper has been implemented using the free software environment R [54] and several contributed packages: `gstat` [55] and `sp` [56] for the geostatistical analysis, `optimx` [57] for the calibration of models, `solaR` [58] for the solar geometry, `raster` [59] for spatial data manipulation and analysis, and `rasterVis` [60] for spatial data visualization methods.

3.2. Methodology of model development

The evaluation of variable importance leads to improve the performance of a general model with specific relationships between predictors and outcomes of the site to be assessed. This evaluation is performed by means of a *loess* smoother fit model, also known as locally weighted polynomial regression, which is fitted between the outcome and the predictors [61]. Each point (x) of the dataset is fitted with a low-degree polynomial. The polynomial is adjusted with weighted least squares, giving more weight to points near the point whose response is being estimated and less weight to points further away. The weights are determined by their distance from x with the tricubic weight function (Equation 3).

$$\omega(x) = (1 - \left|x^3\right|) \tag{4}$$

Eventually, the R^2 is calculated for this model against the intercept only null model. The R^2 is returned as a relative measure of variable importance.

The evaluation is performed with typically used variables such as P, M and ΔT and other two non-commonly used variables W and H of the study day (i) and of three days, two days and the day before ($i-3, i-2, i-1$) and after ($i+3, i+2, i+1$). Those variables with high R^2 are useful to improve the estimation of R_s within a classic model, such as the BC. As a result, new BC-derived models are built according to Equations 5 & 6 with those important variables and then evaluated according to Section 3.1.

$$R_s = a\left(1 - \exp\left(-b \cdot \Delta T^c\right)\right) R_a \cdot A + p_{n+1} \tag{5}$$

$$A = 1 + \sum_{j=1}^{n} p_j \cdot v_j \tag{6}$$

Where, A is the adjustment of the BC model according to the evaluation of variable importance, p is the parameter related to the variable v and n is the number of variables of adjustment.

4. Results and discussion

4.1. Model building

The evaluation of variable importance for La Rioja is collated in Table 3. ΔT, H, and M show values of R^2 higher than 0.15. Throughout the analysis of variable importance it might be proved that rainfall in this region should be explained with M instead of P (0.153 vs. 0.056), which however, is implemented in models 6 and 7. As a result, P is rejected as a variable to explain R_s. Equation 6 might be fitted with different combinations of variables (p_j) and therefore, different models might be built and then evaluated as per Section 3.1. Two different sets of models are built regarding inputs used. The first set of models, constituted by 9 models, is built considering commonly registered meteorological variables (T_{max}, T_{min} and M). The second set of models also integrates W and H and is composed by 3 different models. Since ΔT is already considered within the BC model, only $\Delta T_{j \neq 1}$ are considered in A. Eventually, only p_j and $p_{j \pm 1}$ are relevant in R_s, showing lower errors in the evaluation. M_j, $M_{j \pm 1}$, ΔT_j and $\Delta T_{j \pm 1}$ provide information about the cloud coverage [23] and W and H refine the sky clearness. However, $H_{j \neq 1}$ and $W_{j \neq 1}$ reduce the robustness of models and increase errors. M, M_{i-1} and M_{i+1} were already implemented in the [29] models (models 18 and 19). Equations 6 and 7 show the final models proposed for both afore-mentioned sets.

$$R_s = R_a \cdot a \left(1 - \exp\left(-b \cdot \Delta T^c\right)\right) \cdot \left(1 + d \cdot M_{j-1} + e \cdot M_j + f \cdot M_{j+1} + g \cdot \Delta T_{j+1} + h \cdot \Delta T_{j-1}\right) + l \tag{7}$$

$$R_s = R_a \cdot a \left(1 - \exp\left(-b \cdot \Delta T^c\right)\right) \cdot \left(1 + d \cdot M_{j-1} + e \cdot M_j + f \cdot M_{j+1} + g \cdot \Delta T_{j+1} + h \cdot \Delta T_{j-1} + l \cdot W_j + m \cdot H_j\right) + n \tag{8}$$

4.2. Evaluation of parametric models

The results of the robustness assessment are collated in Figure 2, showing the 95% confidence intervals (95% C.I., n=100) of the MAE_{val} obtained by bootstrapping and also the test errors (MAE_{tes}). Narrow confidence intervals and low values of MAE_{val} imply both stability and accuracy in models, and low MAE_{tes} means high capacity for generalization within the *testing* period. Several models, such as 12 and 13 at station *1*, 12-14 at station *8*, 10 and 12 at the station *12*, and 1-5, 7-10, 12 and 20 at the station *17* among others, generate wide confidence intervals and high values of MAE_{val} and at the same time low MAE_{tes}. In spite of the high capacity for generalization of the afore-mentioned models within the *testing* period, the methodology proposed leads to their selection being avoided. For instance, stable and accurate models such as 24 should be selected at station *17* instead of model 20, although the latter generates lower MAE_{tes}. The robustness assessment is found useful when only short and biased time series are available to evaluate models.

The stability of models is assessed through the $\overline{R_{MAE,val}}$ of the model for the whole set of stations (Table 4). The proposed models (models 23 and 24) improve the results of [29] (models 18 and 19) with $\overline{R_{MAE,val}}$ of 0.360 and 0.261 MJ/m^{2}day and 0.387 and 0.385 MJ/m^{2}day, respectively. Therefore, model 23 is considered the most stable for this region by means of rainfall and daily range of temperatures. However, a significant improvement in stability is achieved introducing W and H in addition to ΔT and M, as seen with model 24. Models 1-10, 15, 20 and 22 generate similar $\overline{R_{MAE,val}}$ between [0.42-0.45] MJ/m^{2}day, and models 12-14, 17 and 21 between [0.48-0.53] MJ/m^{2}day. The low stability of models 11 and 16, with $\overline{R_{MAE,val}}$ of 0.761 and 0.764 MJ/m^{2}day, might be explained by the inclusion of $R_{a,i-30}$ and the lack of R_a, respectively.

Model accuracy is assessed via the average of MAE_{val} for the whole set of stations ($\overline{MAE_{val}}$). The highest accuracy in predictions is also achieved with models 24, 23 and 18 with $\overline{MAE_{val}}$ of 2.195, 2.247 and 2.317 MJ/m^{2}day (Table 4). In addition, model 23 and 24 obtain the lowest values of MAE_{val} of 1.886 ± 0.161 and 1.887 ± 0.090 (95% C.I., n=100) MJ/m^{2}day (Figure 2) at station *11* (*Calahorra*). According to the $t - test$ the MAE_{val} mean is statistically lower in model 24 than any other model in all stations, except in station *9*, in which models 18, 19 and 23 have lower MAE_{val} mean (Table 5). From this test, it can also be deduced that model 23 has statistically lower MAE_{val} than models 18 and 19 in all stations.

The original BC model (model 8) achieves lower $\overline{MAE_{val}}$ (2.617 $\mathrm{MJ/m^2day}$) than other BC-derived models such as 10-14 and 20-21. Models 3, 5 and 6, derived from [9] (model 1), obtain lower $\overline{MAE_{val}}$ than the initial model. [10] (model 7), derived from [22] (model 15) improves the $\overline{MAE_{val}}$ from 2.719 $\mathrm{MJ/m^2day}$ (model 15) to 2.534 $\mathrm{MJ/m^2day}$ (model 7). [30] and [31] models (models 16 and 17), in which ΔT is not considered, achieve $\overline{MAE_{val}}$ of 6.315 $\mathrm{MJ/m^2day}$ and 3.405 $\mathrm{MJ/m^2day}$. [38] (model 11) generates a MAE_{val} of 4.426 $\mathrm{MJ/m^2day}$, due to its high dependency on the $R_{a,i-30}$.

The capacity of generalization of models to non-common days is assessed through the $\overline{RMSE_{val}}$ and $\overline{R_{RMSE,val}}$ in Table 4. The model proposed (model 24) behaves with lower $\overline{RMSE_{val}}$ (2.879 $\mathrm{MJ/m^2day}$) than the other models analyzed and also with a lower $\overline{R_{RMSE,val}}$ (0.361 $\mathrm{MJ/m^2day}$). This model generates lower median of $RMSE_{val}$ in all stations, except in station *9*, in which is lower in models 18, 19 and 23.

Eventually, the models 24 (model proposed by means of ΔT, M, W and H) and model 23 (model proposed by means of ΔT and M) are considered the most suitable models for estimating R_s in La Rioja. Notwithstanding, the model evaluation is focused on model 24 due to its superior stability and accuracy. 41.65% of the daily residuals in the case of SIAR and 20.12% in that of SOS Rioja fall within the uncertainty tolerance of the pyranometers of the two networks (10% and 5%, respectively). However, smaller differences between $R_{s,meas}$ and $R_{s,est}$ are found in Figure 4 when considering yearly sums of R_s. Yearly sums of R_s fall within the uncertainty tolerance of the pyranometers in all estations during the five years (2007-2011) with a higher divergence of 4.823% in 2011. Regarding the relative differences between measured and estimated monthly sums of R_s in 2011, 91.7% and 45.8% of the cases in SIAR and SOS Rioja stand within the tolerance of pyranometers.

The performance of the whole set of models is related to elevation, as shown in Figure 5, with higher MAE_{val} being produced at higher altitudes, as evidenced at stations over 1000 m. A suitable explanation of this behabiour might be because there is more meteorological variability in the mountainous areas of La Rioja, than in the lowlands [26]. A slight correlation with elevation is found in models 10, 14 18-20, 23 and 24, not as marked as with other models.

Figure 6 shows the parameters calibrated on model 24 to estimate R_s in Wh/m^2day. High variability between stations is found within the non explanatory constant (parameter n). This variability was also reported by [29] and might be explained by the strong site dependency described by [26, 62]. [23] and [19] described correlations between the parameters and the distance between stations or latitude and longitude. Nevertheless, no correlation between the values of the parameters and latitude, longitude, elevation or distance between stations is found in model 24.

The effect of rain in model 24 is shown in Figure 7, in which the MAE of non-rainy days is on average 11.3% lower than that of rainy days for the whole set of stations. This is also widely found in the rest of the models, and is explained by the fact that solar irradiation is more complex on rainy and overcast days [10]. 2011 was an especially dry year in La Rioja, with 19.7% less rainfall than the average for the *calibration* period 2007-2010 (Table 2), so the MAE_{tes} figures are significantly low in comparison with the confidence intervals of the MAE_{val} in Figure 2. However, this tendency is broken with some models at station *14* (*Moncalvillo*), where the MAE_{tes} are higher than the MAE_{val}. More cloud cover in the *testing* period, evidenced by $\overline{\Delta T_t}$ being lower that the $\overline{\Delta T_c}$ seen in Table 2 at station *18*, might explain this finding [23].

4.3. Evaluation compared with CM SAF

The mean MAE registered by CM SAF related to $R_{s,meas}$ is 1.983 $\mathrm{MJ/m^2day}$ with a standard deviation of 0.517 $\mathrm{MJ/m^2day}$, in average 10.7% lower than $\overline{MAE_{val}}$ from model 24, although in stations *9*, *11*, *14*, *16* and *17* MAE_{CMSAF} is higher than the confidence interval (95% C.I., n=100). The $RMSE_{CMSAF}$ is 3.207 MJ/m^{2}day with a standard deviation of 0.449 MJ/m^{2}day, being higher than the confidence interval (95% C.I., n=100) in stations *6*, *7*, *9*, *12*, *14*, *16* and *17*. Table 6 shows the errors of testing (*testing* dataset) for the model 24 and CM SAF. It might be deduced that CM SAF generally performs with lower errors than model 24 except in stations *9*, *11*, *14*, *16* and *17* (same stations with lower MAE_{val} and $RMSE_{val}$ than CM SAF), in which model 24 is superior.

Figure 3 shows the performance of model 24 with new data from the testing database. This model achieves coefficients of determination (R^2) with linear regression of [0.87-0.91] and [0.79-0.87] for stations below and above 1000 m respectively. The coefficients of determination from CM SAF against $R_{s,meas}$ (R^2_{CMSAF}) are significantly higher than R^2, but also showing a relation with elevation, being lower at higher elevation.

The annual irradiation estimated by CM SAF is significantly higher than the $R_{s,meas}$, which was also found in Spain by [63]. Stations *11*, *14*, *16* and *17* present relative differences substantially above the tolerance of pyranometers reaching 22.95% in station *14* in year 2011. Thus, the model proposed (model 24) is able to estimate more accurately annual irradiation in this region than the CM SAF during years 2007-2011.

It could be argued that, because the CM SAF estimations show higher R^2 values, their worse results in the RMSE and MAE indicators may be improved with a local calibration. This approach was developed in [63] with a geostatistical interpolation (kriging with external drift) using data from a network of 301 ground stations and also CM SAF. A more simplified approach is to use a parametric model as Equation 9,

$$R_s = R_a \cdot (a \cdot \frac{R_{s,cmsaf}}{R_a} + b) \tag{9}$$

where the CMSAF estimations are normalized with the extraterrestial radiation and calibrated with the on-ground radiation measurements. This approach has been analyzed achieving $\overline{MAE_{val}}$ and $\overline{RMSE_{val}}$ of 1.913 and 2.987 MJ/m^{2}day with $\overline{R_{MAE,val}}$ and $\overline{R_{RMSE,val}}$ of 0.422 and 0.886 MJ/m^{2}day, respectively. The R^2 in this parametrization is also lowered respect the actual R^2 of CM SAF. This means that it is only improved the $\overline{MAE_{val}}$ respect to the model 24 while getting the other indicators worse. However, this re-calibration of CM SAF leads to lower errors in annual sums of global irradiation with CM SAF (in 15 stations the error is within the 5% and a 5.7% maximum error). The Table 7 shows parameters of Equation 9, where a_{mean}, b_{mean}, a_{sd}, b_{sd} are the average and standard deviations of a and b.

5. Conclusions

The methodology proposed of model development of adjusting a general model with the on-site peculiarities based on the evaluation of variable importance is proved appropiated within the case study of La Rioja region (northern Spain). The high site dependency of R_s related to the meteorological trends suggests the adjustment of general parametric models (such as the *BC* and [9] models) with those variables that show higher correlation with R_s. By means of this methodology, different models might be proposed in locations with different climates. The new model includes M, M_{i-1}, M_{i+1}, ΔT_{i-1}, ΔT_{i+1}, W, H as explanatory variables (derived from the evaluation of variable importance) that adjust the *BC* model in La Rioja.

The methodology proposed of model evaluation is based on bootstrapping and proves useful in selecting models according to stability and accuracy and not only based on test errors. The proposed model is evaluated with this methodology against a review of twenty-two already existing parametric models at seventeen meteorological stations within La Rioja. The new model improves the estimates of the other twenty-two models with $\overline{MAE_{val}}$ of 2.195 MJ/m^{2}day and

$\overline{R_{MAE,val}}$ of 0.261 MJ/m^{2}day. However, several BC derived models (10-14, 20-21) fail to improve the estimates of the original model. This might be explained because these models include variables that do not show high correlation with R_s (such as P) within La Rioja. In addition, significant differences in stability between models and meteorological stations are recorded with these models. The performance of the model proposed is compared with $R_{s,CMSAF}$, obtaining lower confidence interval (95% C.I., n=100) of MAE_{val} than MAE_{CMSAF} in 5 stations and for $RMSE_{val}$ in 7 stations.

Rainfall and elevation are shown to influence the accuracy of model performance (generating higher errors in rainy days and also at higher stations). The fact that the *testing* dataset (year 2011) was significantly drier than the *calibration* dataset (years 2007-2010) explains the low MAE_{tes} recorded.

The residuals of estimates are found to have yearly periodicity, with higher relative residuals when meteorological variability is greater. 41.65% of the daily residuals in the case of SIAR and 20.12% in that of SOS Rioja fall within the uncertainty tolerance of the pyranometers of the two networks (10% and 5%, respectively). However, the annual relative differences between $R_{s,meas}$ and $R_{s,est}$ are lower than 4.82%, which means that estimates are within the confidence interval of pyranometers.

The analysis of parametric models against the CM SAF satellite-derived irradiation data shows that the mean MAE_{CMSAF} is in average 10.7% lower than $\overline{MAE_{val}}$, but also that in 5 stations the $\overline{MAE_{val}}$ is significantly lower than the one of CM SAF. This tendence is also common with the $RMSE$, which is generally lower with CM SAF, but not always (7 stations). Nevertheless, attending to the annual irradiation it has been proved that the model proposed (model 24) achieves significantly better estimates that the CM SAF, which over-estimates solar irradiation within the region studied. The possibility of shades on the positions of stations over the CM SAF estimates has been previously analyzed and rejected. As a result, the proposed model might be useful to estimate annual sums of R_s, reaching insignificant differences with R_s from pyranometers and also to be used on a daily basis when correctly calibrated with on-ground data.

Acknowledgements

We are indebted to the University of La Rioja (fellowship FPI 2012) and the Research Institute of La Rioja (IER) for funding parts of this research.

References

[1] Running, S. W., Nemani, R. R., Hungerford, R. D., 1987. Extrapolation of synoptic meteorological data in mountainous terrain and its use for simulating forest evapotranspiration and photosynthesis. Can. J. For. Res. 17, 472–483.

[2] Crop Growth Monitoring System
URL http://www.marsop.info/marsopdoc/cgms92/2_2_2_en.htm

[3] Beyer, H. G., Polo-Martinez, J., Suri, M., Torres, J. L., Lorenz, E., Muller, S. C., Hoyer-Klick, C., Ineichen, P., 2009. Mesor: Management and exploitation of solar resource knowledge. D 1.1.3 Report on Benchmarking of Radiation Products., 1–160.

[4] Schulz, J., Albert, P., Behr, H.-D., Caprion, D., Deneke, H., Dewitte, S., Dürr, B., Fuchs, P., Gratzki, A., Hechler, P., Hollmann, R., Johnston, S., Karlsson, K.-G., Manninen, T., Müller, R., Reuter, M., Riihelä, A., Roebeling, R., Selbach, N., Tetzlaff, A., Thomas, W., Werscheck,

M., Wolters, E., Zelenka, A., 2009. Operational climate monitoring from space: the EUMETSAT satellite application facility on climate monitoring (CM-SAF). Atmos. Chem. Phys. 9 (5), 1687–1709.

[5] Posselt, R., Mueller, R., Stockli, R., Trentmann, J., 2012. Remote sensing of solar surface radiation for climate monitoring - the CM-SAF retrieval in international comparison. Remote Sens. Environ. 118 (0), 186 – 198.

[6] Rahimikhoob, A., 2010. Estimating global solar radiation using artificial neural network and air temperature data in a semi-arid environment. Renew. Energ. 35 (9), 2131 – 2135.

[7] Senkal, O., 2010. Modeling of solar radiation using remote sensing and artificial neural network in Turkey. Energy 35 (12), 4795 – 4801.

[8] Bristow, K. L., Campbell, G. S., 1984. On the relationship between incoming solar radiation and daily maximum and minimum temperature. Agric. For. Meteorol. 31 (2), 159 – 166.

[9] Hargreaves, G. H., 1981. Responding to tropical climates. In: 1980-81 Food and Climate Review. The Food and Climate Forum. Aspen Institue for Humanistic Studies, Boulder, Colorado, pp. 29–32.

[10] Jong, R. D., Stewart, D. W., 1993. Estimating global solar radiation from common meteorological observations in western Canada. Can. J. Plant Sci. 73 (2), 509–518.

[11] The Satellite Application Facility on Climate Monitoring (CM SAF)
URL http://www.cmsaf.eu

[12] SODA
URL http://www.soda-is.com/eng/index.html

[13] INPE
URL http://www.inpe.br

[14] National and Renewable Energy Laboratory (NREL)
URL http://www.nrel.gov/gis/solar.html

[15] NASA Surface meteorology and Solar Energy (SSE)
URL http://maps.nrel.gov/SWERA

[16] Perez, R., Seals, R., Stewart, R., Zelenka, A., Estrada-Cajigal, V., 1994. Using satellite-derived insolation data for the site/time specific simulation of solar energy systems. Solar Energy 53 (6), 491-495.

[17] Angstrom, A., 1924. Solar and terrestrial radiation. Report to the international commission for solar research on actinometric investigations of solar and atmospheric radiation. Q. J. Roy. Meteor. Soc. 50 (210), 121–126.

[18] Prescott, J., 1940. Evaporation from a water surface in relation to solar radiation. Trans. R. Soc. So. Augst. 64, 114–125.

[19] Liu, X., Mei, X., Li, Y., Wang, Q., Jensen, J. R., Zhang, Y., Porter, J. R., 2009. Evaluation of temperature-based global solar radiation models in China. Agric. For. Meteorol. 149 (9), 1433 – 1446.

[20] Supit, I., van Kappel, R., 1998. A simple method to estimate global radiation. Sol. Energy 63 (3), 147 – 160.

[21] Ododo, J., 1997. Prediction of solar radiation using only maximum temperature and relative humidity: south-east and north-east Nigeria. Energy Convers. Manage. 38 (18), 1807 – 1814.

[22] Richardson, C. W., 1981. Stochastic simulation of daily precipitation, temperature, and solar radiation. Water Resour. Res. 17 (1), 182–190.

[23] Trnka, M., Zalud, Z., Eitzinger, J., Dubrovsky, M., 2005. Global solar radiation in Central European lowlands estimated by various empirical formulae. Agric. For. Meteorol. 131 (12), 54 – 76.

[24] Allen, R. G., 1995. Evaluation of procedures for estimating mean monthly solar radiation from air temperature. Report. Food and Agricultural Organization of the United Nations (FAO), Rome., Rome.

[25] Allen, R. G., 1997. Self-calibrating method for estimating solar radiation from air temperature. J. Hydrol. Eng. 2 (2), 56–67.

[26] Annandale, J. G., Jovanovic, N. Z., Benade, N., Allen, R. G., Mar. 2002. Software for missing data error analysis of Penman-Monteith reference evapotranspiration. Irrig. Sci. 21 (2), 57 - 67.

[27] Chen, R., Ersi, K., Yang, J., Lu, S., Zhao, W., 2004. Validation of five global radiation models with measured daily data in China. Energy Convers. Manage. 45, 1759 – 1769.

[28] Hunt, L., Kuchar, L., Swanton, C., 1998. Estimation of solar radiation for use in crop modelling. Agric. For. Meteorol. 91, 293 – 300.

[29] Liu, D., Scott, B., 2001. Estimation of solar radiation in Australia from rainfall and temperature observations. Agric. For. Meteorol. 106 (1), 41 – 59.

[30] McCaskill, M., 1990. An efficient method for generation of full climatological records from daily rainfall. Aust. J. Agric. Res. Aust. J. Agric. Res., 595–602.

[31] McCaskill, M., 1990. Prediction of solar radiation from rainday information using regionally stable coefficients. Agric. For. Meteorol. 51, 247–255.

[32] Weiss, A., Hays, C. J., 2004. Simulation of daily solar irradiance. Agric. For. Meteorol. 123, 187 – 199.

[33] Meza, F., Varas, E., 2000. Estimation of mean monthly solar global radiation as a function of temperature. Agric. For. Meteorol. 100, 231 – 241.

[34] Prieto, J., Martínez-García, J., García, D., 2009. Correlation between global solar irradiation and air temperature in Asturias, Spain. Sol. Energy 83 (7), 1076 – 1085.

[35] Abraha, M., Savage, M., 2008. Comparison of estimates of daily solar radiation from air temperature range for application in crop simulations. Agric. For. Meteorol. 148 (3), 401 – 416.

[36] Donatelli, M., Campbell, G., 1998. A simple model to estimate global solar radiation. In: Proc. ESA Cong., 5th, Nitra, Slovak Republic, 28 June- 2 July, 1998. The Slovak Agriculture University, 133–134.

[37] Goodin, D. G., Hutchinson, J. M. S., Vanderlip, R. L., Knapp, M. C., 1999. Estimating solar irradiance for crop modeling using daily air temperature data. Agron. J. 91 (5), 845–851.

[38] Weiss, A., Hays, C. J., Hu, Q., Easterling, W. E., 2001. Incorporating bias error in calculating solar irradiance: Implications for crop yield simulations. Agron. J. 93 (6), 1321–1326.

[39] Almorox, J., Hontoria, C., Benito, M., 2011. Models for obtaining daily global solar radiation with measured air temperature data in Madrid (Spain). Appl. Energ. 88 (5), 1703 – 1709.

[40] Mavromatis, T., Jagtap, S. S., 2005. Estimating solar radiation for crop modeling using temperature data from urban and rural stations. Climate Res. 29 (3), 233–243.

[41] Thornton, P. E., Running, S. W., 1999. An improved algorithm for estimating incident daily solar radiation from measurements of temperature, humidity, and precipitation. Agric. For. Meteorol. 93 (4), 211 – 228.

[42] Winslow, J. C., Hunt, E. R., Piper, S. C., 2001. A globally applicable model of daily solar irradiance estimated from air temperature and precipitation data. Ecol. Model. 143 (3), 227 – 243.

[43] Korpela, M., Mäkinen, H., Nöjd, P., Hollmén, J., Sulkava, M., Jun. 2010. Automatic detection of onset and cessation of tree stem radius increase using dendrometer data. Neurocomputing 73, 2039–2046.

[44] Sos Rioja
URL http://www.larioja.org/npRioja/default/defaultpage.jsp?idtab=441001

[45] Siar
URL http://ias1.larioja.org/estaciones/estaciones/siar/portada/index.jsp

[46] Lawrence, S., Giles, C. L., Tsoi, A. C., 1996. What size neural network gives optimal generalization? Convergence properties of backpropagation. Technical Report UMIACS-TR-96-22 and CS-TR-3617. Institute for Advanced Computer Studies. University of Maryland College Park, MD 20742, 1–35.

[47] Crawley, M. J., 2005. Statistics: an introduction using R. John Wiley.

[48] Mora, J., Mora-López, L., 2010. Comparing distributions with bootstrap techniques: An application to global solar radiation. Math. Comput. Simulat. 81 (4), 811 – 819.

[49] Varadhan, R., 2012. BB: Solving and optimizing large-scale nonlinear systems, r package version 2012.3-1 (2012).
URL URLhttp://cran.r-project.org/web/packages/BB/BB.pdf

[50] Broyden, C. G., 1970. The convergence of a class of double-rank minimization algorithms. General considerations. IMA J. Appl. Math. 6 (1), 76–90.

[51] Nielsen, H., Mortensen, S., 2007. ucminf: General-purpose unconstrained non-linear optimization.
URL http://CRAN.R-project.org/package=ucminf

[52] Willmott, C. J., Matsuura, K., 2005. Advantages of the mean absolute error (MAE) over the root mean square error (RMSE) in assessing average model performance. Climate Res. 30 (1), 79–82.

[53] Moreno, A., Gilabert, M., Martínez, B., 2011. Mapping daily global solar irradiation over Spain: A comparative study of selected approaches. Sol. Energy 85 (9), 2072 – 2084.

[54] R Development Core Team, 2012. R: A language and environment for statistical computing. R Foundation for Statistical Computing, Vienna, Austria, ISBN 3-900051-07-0.
URL http://www.R-project.org

[55] Pebesma, E. J., 2004. Multivariable geostatistics in s: the gstat package. Comput. Geosci. 30, 683–691.

[56] Pebesma, E. J., Bivand, R. S., November 2005. Classes and methods for spatial data in R. R News 5 (2), 9–13.
URL http://CRAN.R-project.org/doc/Rnews/

[57] Nash, J. C., Varadhan, R., 2012. optimx: A replacement and extension of the optim() function.
URL http://cran.r-project.org/web/packages/optimx/index.html

[58] Perpiñán, O., 2012. solaR: Solar radiation and photovoltaic systems with R. J. Stat. Softw. 50 (9), 1–32.
URL http://www.jstatsoft.org/v50/i09/

[59] Hijmans, R. J., van Etten, J., 2012. raster: Geographic analysis and modeling with raster data.
URL http://cran.r-project.org/web/packages/raster/

[60] Perpiñán, O., Hijmans, R., 2012. rasterVis: Visualization methods for the raster package. R package version 0.10-9.
URL http://CRAN.R-project.org/package=rasterVis

[61] Cleveland, W., 1979. Robust locally weighted regression and smoothing scatterplots. Journal of the American Statistical Association 74 (368): 829–836.

[62] Gueymard, C., Jindra, P., Estrada-Cajigal, V., 1995. A critical look at recent interpretations of the Angstrom approach and its future in global solar radiation prediction. Sol. Energy 54 (5), 357 – 363.

[63] Antonanzas-Torres, F., Cañizares, F., Perpiñán, O., 2013. Comparative assessment of global irradiation from a satellite estimate model (CM SAF) and on-ground measurements (SIAR): a Spanish case study. Renew. Sust. Energ. Rev. 21 248-261.

Model no.	Equation	Parameters	Authors
1	$R_s = a\sqrt{\Delta T} R_a$	a	[9]
2	$R_s = a\left(1 + 2.7 \cdot 10^{-5} \cdot h\right) \sqrt{\Delta T} R_a$	a	[26]

Continued on next page

Model no.	Equation	Parameters	Authors
3	$R_s = \left(a\sqrt{\Delta T} + b\right) R_a$	a, b	[27]
4	$R_s = (a \cdot \ln(\Delta T) + b) R_a$	a, b	[27]
5	$R_s = a\sqrt{\Delta T} R_a + b$	a, b	[28]
6	$R_s = a\sqrt{\Delta T} R_a + b \cdot T_{max} + c \cdot P + d \cdot P^2 + e$	a, b, c, d, e	[28]
7	$R_s = a \cdot R_a \cdot \Delta T^b \left(1 + c \cdot P + d \cdot P^2\right)$	a, b, c, d	[10]
8	$R_s = a(1 - \exp(-b \cdot \Delta T^c)) R_a$	a, b, c	[8]
9	$R_s = a \cdot R_a \left(1 - \exp\left(-b\sqrt{\Delta T} - c \cdot \Delta T - d \cdot \Delta T^2\right)\right)$	a, b, c, d	[28]
10	$R_s = a\left(1 - \exp\left(-b\frac{\Delta T^c}{R_a}\right)\right) R_a$	a, b, c	[37]
11	$R_s = a\left(1 - \exp\left(-b\frac{\Delta T^c}{R_{a,i-30}}\right)\right) R_a$	a, b, c	[38]
12	$R_s = 0.7\left(1 - \exp\left(-b \cdot \Delta T^{2,4}\right)\right) R_a$	b	[33]
13	$R_s = 0.75\left(1 - \exp\left(-b \cdot \Delta T^2\right)\right) R_a$	b	[19]

Continued on next page

Model no.	Equation	Parameters	Authors
14	$$R_s = 0.75\left(1-\exp\left(-b\cdot\frac{\Delta T^2}{\Delta T_m}\right)\right)R_a$$	b	[19]
15	$$R_s = \left(a\cdot\Delta T^b\right)R_a$$	a, b	[22]
16	$$\begin{aligned}R_s = a + b\cdot\cos(\theta) + c\cdot\sin(\theta)\\ + d\cdot\cos(2\theta) + e\cdot\sin(2\theta)\\ + f\cdot M_{j-1} + g\cdot M_j + h\cdot M_{j+1}\end{aligned}$$	a, b, c, d, e, f, g, h	[30]
17	$$R_s = a\cdot R_a + b\cdot M_{j-1} + c\cdot M_j + d\cdot M_{j+1}$$	a, b, c, d	[31]
18	$$\begin{aligned}R_s = R_a\cdot a\left(1-\exp\left(-b\cdot\Delta T^c\right)\right)\\ \cdot\left(1 + d\cdot M_{j-1} + e\cdot M_j + f\cdot M_{j+1}\right) + g\end{aligned}$$	a, b, c, d, e, f, g	[29]
19	$$\begin{aligned}R_s = R_a\cdot a\left(1-\exp\left(-b\cdot\Delta T^c\right)\right)\\ + d\cdot M_{j-1} + e\cdot M_j + f\cdot M_{j+1} + g\end{aligned}$$	a, b, c, d, e, f, g	[29]
20	$$R_s = a\left(1-\exp\left(-b\frac{\Delta T^c}{\Delta T_m}\right)\right)R_a$$	a, b, c	[36]
21	$$R_s = 0.75\left(1-\exp\left(-b\cdot\Delta T^2\cdot f\left(T_{avg}\right)\right)\right)$$ $$f\left(T_{avg}\right) = 0.017\exp\left(\exp\left(-0.053\cdot T_{avg}\cdot\Delta T\right)\right)$$	b	[36]

Continued on next page

Model no.	Equation	Parameters	Authors
22	$R_s = a \cdot R_a \cdot \Delta T^b (1 - \exp(-c \cdot p_{sat}[T_{max}]))^d$	a, b, c, d	[39]
23	$R_s = R_a \cdot a\,(1 - \exp(-b \cdot \Delta T^c)) \cdot (1 + d \cdot M_{j-1} + e \cdot M_j + f \cdot M_{j+1} + g \cdot \Delta T_{j+1} + h \cdot \Delta T_{j-1}) + l$	a, b, c, d, e, f, g, h, l	Proposed model
24	$R_s = R_a \cdot a\,(1 - \exp(-b \cdot \Delta T^c)) \cdot (1 + d \cdot M_{j-1} + e \cdot M_j + f \cdot M_{j+1} + g \cdot \Delta T_{j+1} + h \cdot \Delta T_{j-1} + l \cdot W_j + m \cdot H_j) + n$	a, b, c, d, e, f, g, h, l, m,n	Proposed model

Table 1: Summary of the twenty-three parametric models studied. ΔT is the difference between T_{max} and T_{min}. $R_{a,i-30}$ is the extraterrestrial irradiation on day *i-30*, h is the elevation above sea level, T_{avg} is the daily average air temperature, ΔT_m is the monthly average of ΔT and $p_{sat}[T_{max}]$ is the vapor saturation pressure at T_{max}

#	Name	Net.	Lat.(º)	Long.(º)	Alt.	$\overline{\Delta T_c}$	$\overline{\Delta T_t}$	P_c	P_t	$\overline{R_{s,c}}$	$\overline{R_{s,t}}$
1	Agoncillo	SIAR	42.46	-2.29	342	12.3	12.6	484	318	14.7	15.3
2	Aldeanueva	SIAR	42.22	-1.90	390	11.1	11.4	405	327	15.4	15.4
3	Alfaro	SIAR	42.15	-1.77	315	12.5	12.9	335	364	15.3	15.2
4	Casalarreina	SIAR	42.53	-2.89	510	11.8	12.4	486	341	14.2	14.2
5	Cervera	SIAR	42.00	-1.89	495	13.9	14.3	356	331	15.2	15.0
6	Foncea	SIAR	42.60	-3.03	669	10.1	10.5	647	422	14.8	14.7
7	Leiva	SIAR	42.49	-3.04	595	11.4	11.5	499	379	14.5	14.4
8	Rincon	SIAR	42.25	-1.85	277	12.3	12.7	393	348	15.3	15.5
9	Urunuela	SIAR	42.46	-2.71	465	11.4	12.4	476	345	14.1	14.2
10	Aguilar	SOS	41.96	-1.96	752	9.3	9.7	463	236	14.5	14.7
11	Calahorra	SOS	42.29	-1.99	350	11.1	11.3	305	250	13.3	13.4
12	Ezcaray	SOS	42.33	-3.00	1000	10.3	10.7	538	381	13.6	13.6
13	Logroño	SOS	42.45	-2.74	408	10.1	10.3	423	212	14.3	14.3
14	Moncalvillo	SOS	42.32	-2.61	1495	7.8	7.7	567	429	12.0	11.9
15	San Roman	SOS	42.23	-2.45	1094	8.2	8.2	323	332	13.9	14.2

#	Name	Net.	Lat.(°)	Long.(°)	Alt.	$\overline{\Delta T_c}$	$\overline{\Delta T_t}$	P_c	P_t	$\overline{R_{s,c}}$	$\overline{R_{s,t}}$
16	Ventrosa	SOS	42.17	-2.84	1565	7.4	7.7	447	412	12.2	12.1
17	Villoslada	SOS	42.12	-2.66	1235	9.7	9.9	499	325	12.6	12.4

Table 2: Summary of the seventeen meteorological stations. $\overline{\Delta T_c}$ and $\overline{\Delta T_t}$ are the average ΔT of the *calibration* and *testing* datasets, respectively. P_c is the yearly average rainfall in mm for the *calibration* dataset and P_t is the yearly rainfall for the *testing* dataset. $\overline{R_{s,c}}$ and $\overline{R_{s,t}}$ are the daily average R_s for the *calibration* and *testing* datasets, respectively

v	P_i	P_{i+1}	P_{i-1}	M_i	M_{i+1}	M_{i-1}	ΔT_i	ΔT_{i+1}	ΔT_{i-1}	ΔT_{i+2}	ΔT_{i-2}
R^2	0.056	0.012	0.016	0.153	0.068	0.059	0.533	0.359	0.340	0.301	0.172

v	ΔT_{i+3}	ΔT_{i-3}	W_i	W_{i+1}	W_{i-1}	H_i	H_{i+1}	H_{i-1}	H_{i+2}	H_{i-2}
R^2	0.206	0.167	0.089	0.076	0.071	0.465	0.344	0.251	0.251	0.199

Table 3: Summary of variable importance results related to each variable v

Model	1	2	3	4	5	6	7	8	9	10	11	12
$\overline{MAE_{val}}$	2.814	2.809	2.699	2.679	2.797	2.768	2.534	2.617	2.613	2.791	4.426	2.791
$\overline{R_{MAE,val}}$	0.436	0.415	0.426	0.425	0.411	0.430	0.420	0.420	0.422	0.423	0.761	0.527
$\overline{RMSE_{val}}$	3.572	3.560	3.475	3.448	3.541	3.488	3.409	3.294	3.398	3.584	5.873	3.825
$\overline{R_{RMSE,val}}$	0.559	0.545	0.601	0.569	0.549	0.539	0.577	0.605	0.593	0.579	0.996	0.745

Model	13	14	15	16	17	18	19	20	21	22	23	24
$\overline{MAE_{val}}$	2.804	2.751	2.719	6.273	3.366	2.317	2.336	2.678	2.728	2.723	2.247	2.195
$\overline{R_{MAE,val}}$	0.491	0.488	0.444	0.764	0.498	0.387	0.385	0.445	0.498	0.432	0.360	0.261
$\overline{RMSE_{val}}$	3.798	3.708	3.485	7.377	4.256	3.023	3.081	3.457	3.693	3.504	2.995	2.879
$\overline{R_{RMSE,val}}$	0.715	0.691	0.583	0.802	0.649	0.548	0.538	0.606	0.694	0.576	0.543	0.361

Table 4: Summary of statistics in MJ/m^{2}day

Mod. 18	1	2	3	4	5	6	7	8	9	10	11	12	13	14	15	16	17
$p-value$	0.9	0.9	0.9	0.6	0.9	0.8	0.8	0.9	0.0	0.9	0.6	0.9	0.9	0.7	0.9	0.6	0.9
Mod. 23	**1**	**2**	**3**	**4**	**5**	**6**	**7**	**8**	**9**	**10**	**11**	**12**	**13**	**14**	**15**	**16**	**17**
$p-value$	0.9	0.9	0.9	0.9	0.9	0.7	0.4	0.9	0.0	0.9	0.7	0.6	0.9	0.7	0.3	0.6	0.9

Table 5: Summary of $p-values$ of $t-test$ in the MAE_{val} of model 24 against model 18 and model 23 ($p-values$ greater than 0.05 imply statistically significant lower MAE_{val} in model 24)

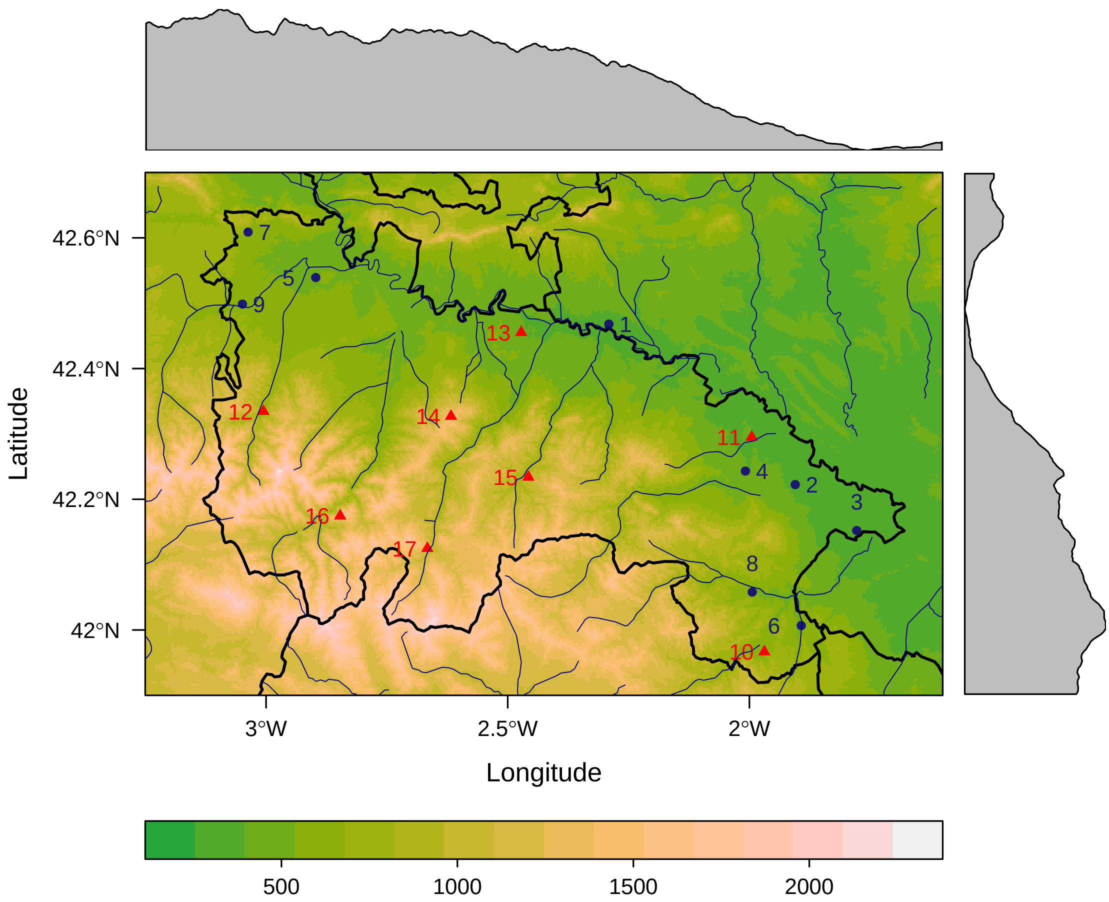

Figure 1: Location of the meteorological stations selected in the region of La Rioja. The color band represents elevation (m). SIAR stations are shown by blue circles and SOS Rioja stations by red triangles

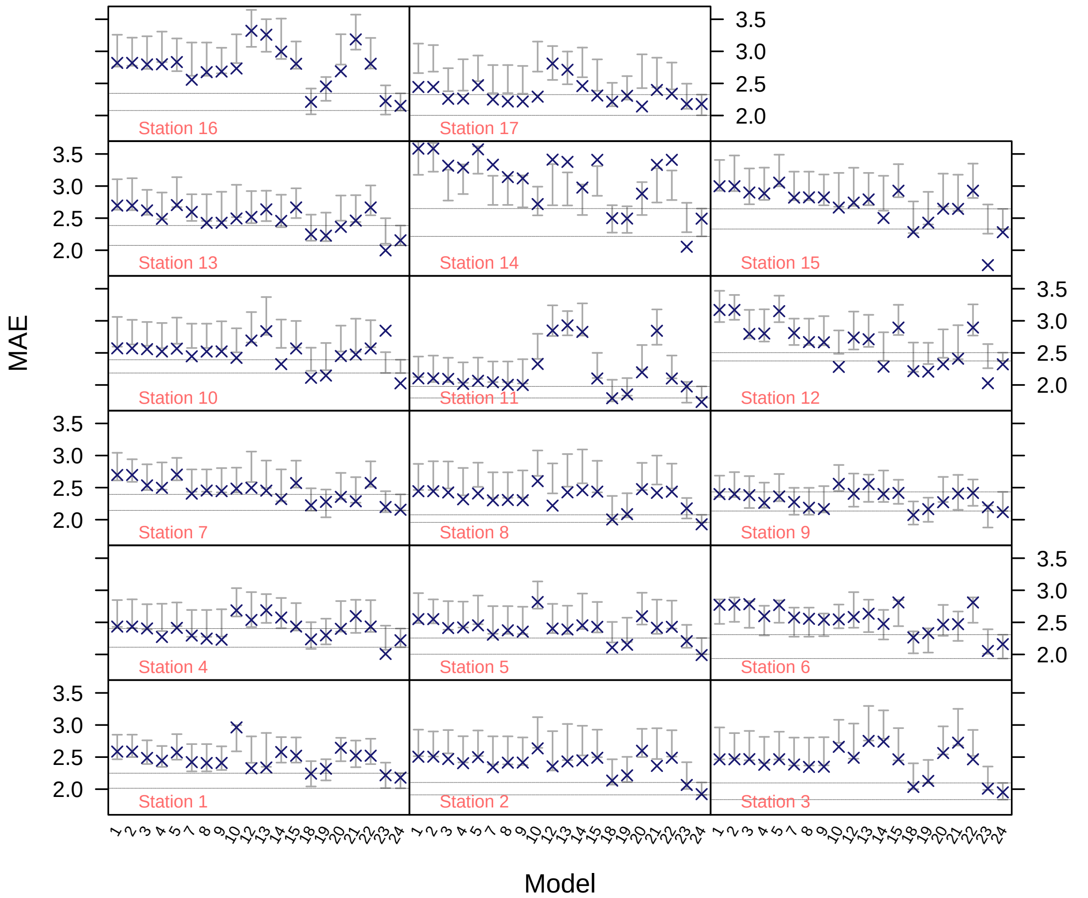

Figure 2: Confidence intervals (95% C.I., n=100) of MAE_{val} (grey vertical lines) and MAE_{tes} (blue crosses) (MJ/m^{2}day). Note that some of the values of models 11, 16 and 17 lie outside the range of the figure

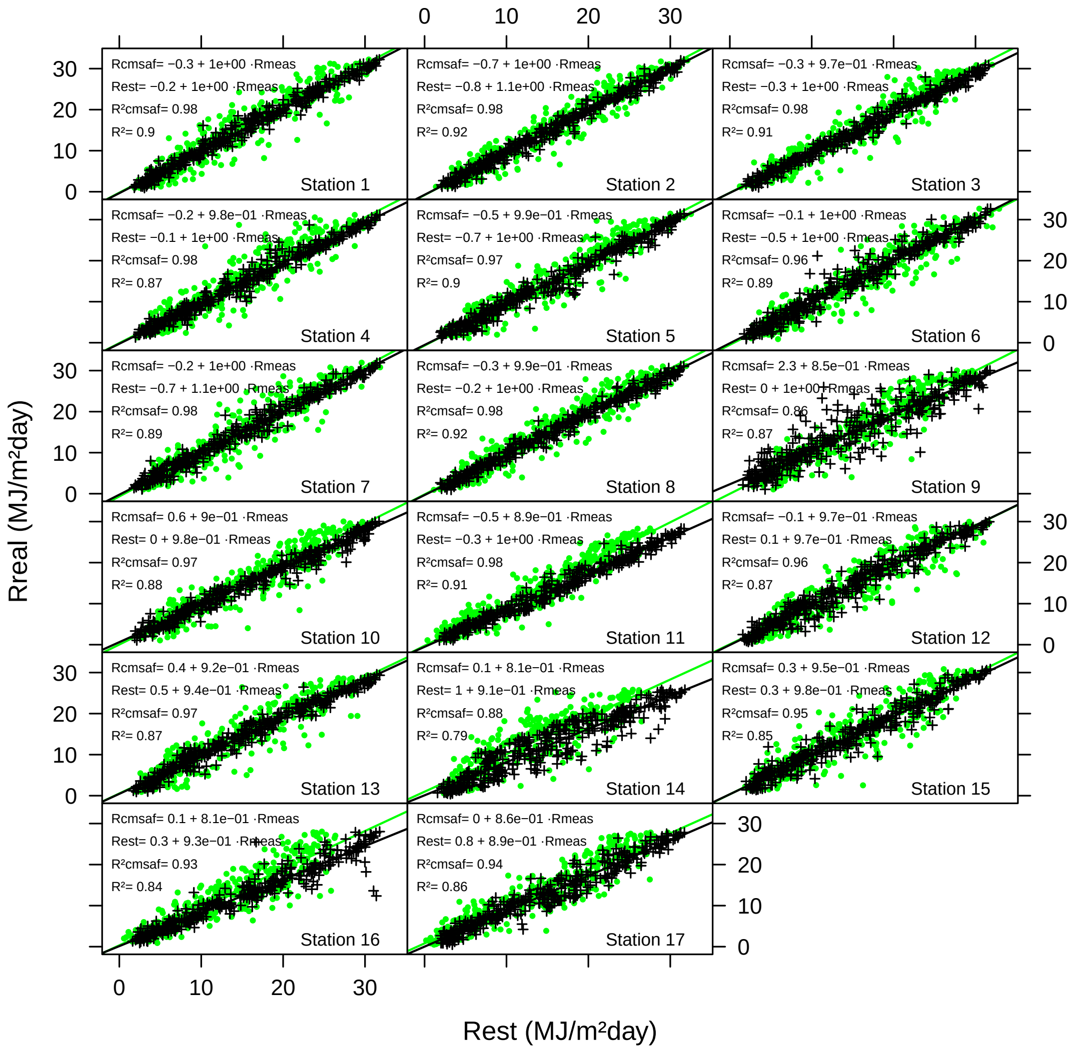

Figure 3: Correlation between $R_{s,meas}$ (MJ/m^2day) and $R_{s,est}$ of the model proposed (model 24) with green points and $R_{s,cmsaf}$ with black crosses within the *testing* time series at all seventeen stations

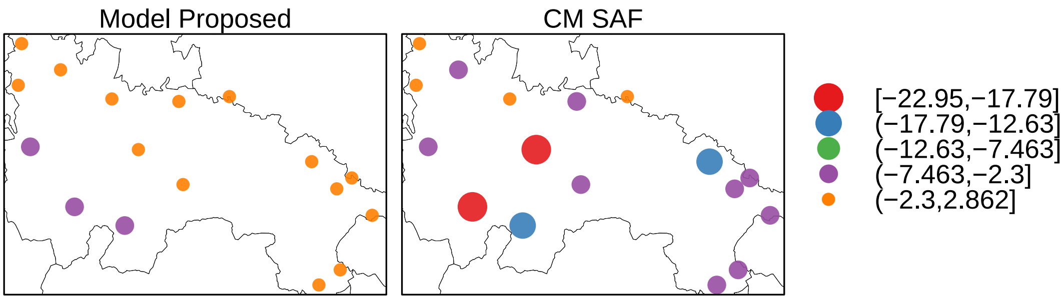

Figure 4: Annual relative difference (%) between $R_{s,meas}$ and $R_{s,est}$ for the model proposed (model 24) and CM SAF during the *testing* period (year 2011).

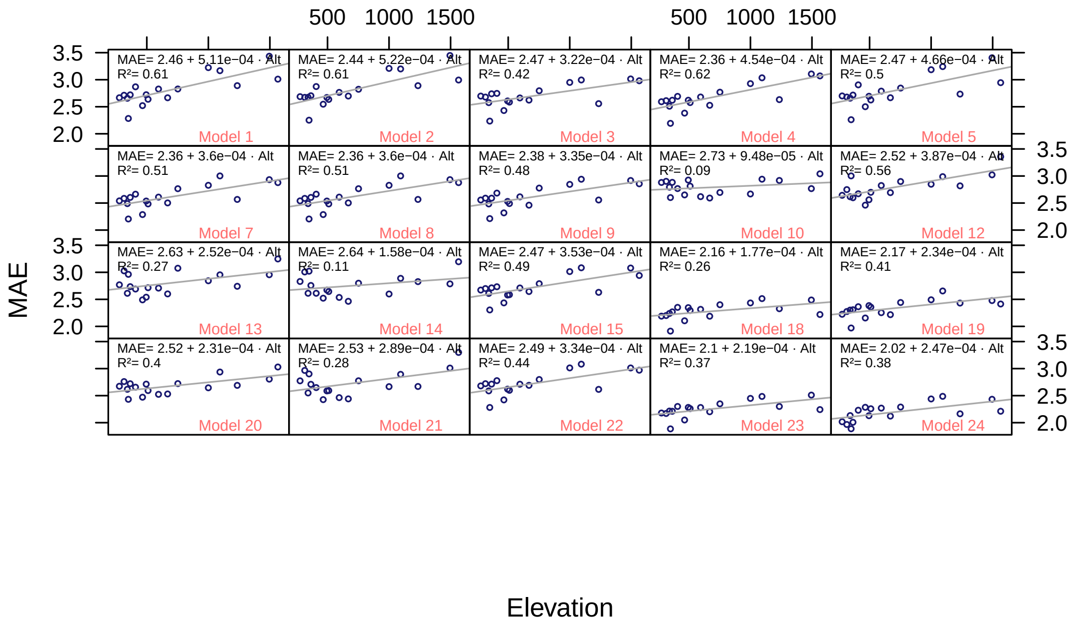

Figure 5: Relation between elevation (m) and median of the MAE_{val} (MJ/m^{2}day). Models 11, 16 and 17 are not shown due to their high MAE_{val}

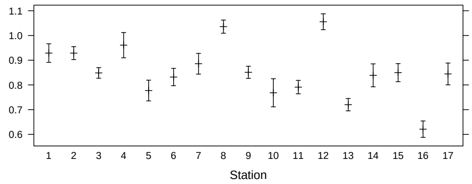

(a) Parameter a

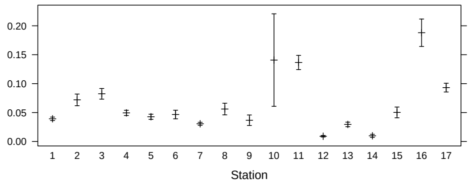

(b) Parameter b

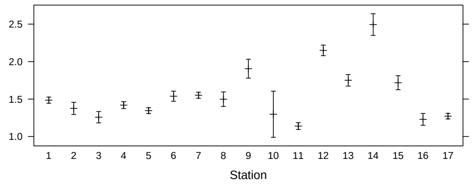

(c) Parameter c

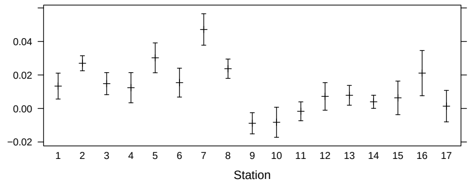

(d) Parameter d

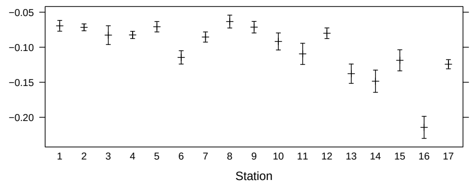

(e) Parameter e

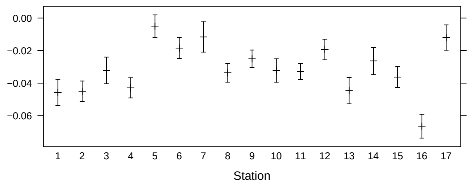

(f) Parameter f

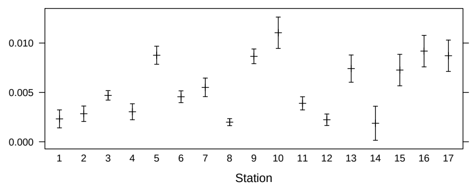

(g) Parameter g

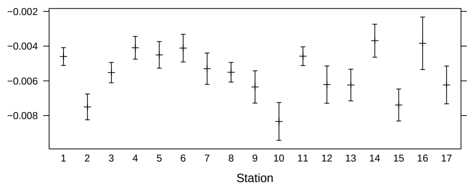

(h) Parameter h

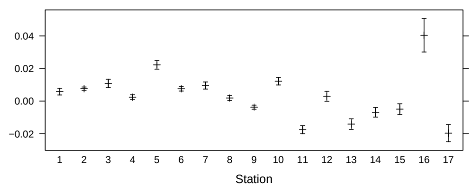

(i) Parameter l

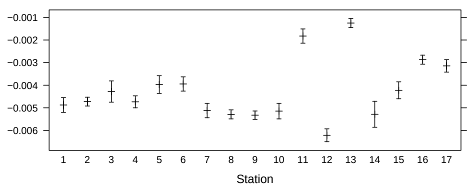

(j) Parameter m

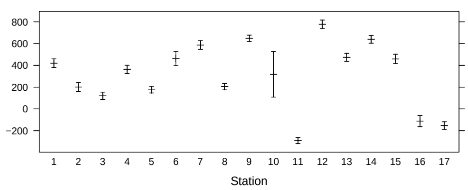

(k) Parameter n

Figure 6: Confidence intervals (95% C.I., n=100) and median of the parameters of the proposed model (model 24)

Station	$MAE_{tes,24}$	$MAE_{tes,CMSAF}$	$RMSE_{tes,24}$	$RMSE_{tes,CMSAF}$
1	2.18	0.91	2.85	1.20
2	1.92	0.86	2.46	1.17
3	1.95	1.05	2.55	1.33
4	2.22	1.09	3.00	1.43
5	1.99	1.12	2.65	1.60
6	2.16	1.13	2.83	1.67
7	2.16	0.95	2.89	1.29
8	1.93	0.93	2.45	1.19
9	2.12	2.27	2.79	3.20
10	2.03	1.37	2.71	1.80
11	1.74	2.35	2.28	2.74
12	2.32	1.34	2.99	1.79
13	2.15	1.30	2.93	1.65
14	2.49	3.18	3.36	4.02
15	2.28	1.32	3.07	1.87
16	2.15	2.83	2.99	3.63
17	2.18	2.28	2.90	2.91

Table 6: Testing errors of model 24 and CM SAF (year 2011)

a_{mean}	a_{sd}	b_{mean}	b_{sd}
0.61	0.05	0.09	0.04

Table 7: Summary of CM SAF re-calibration as per Equation 9

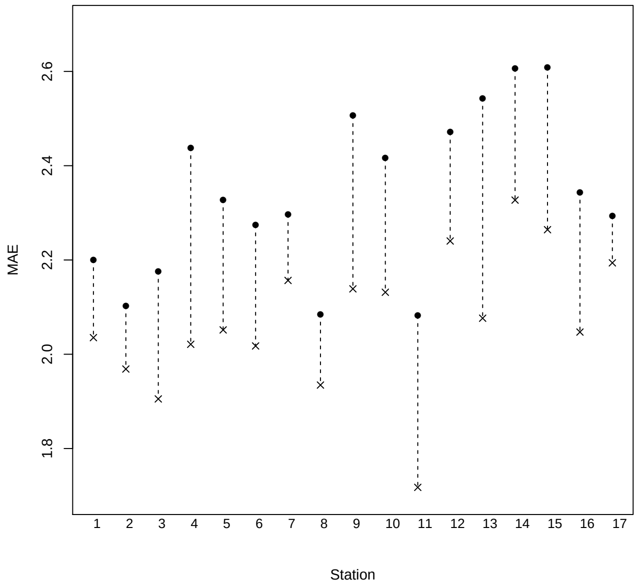

Figure 7: Average MAE (MJ/m^{2}day) of the proposed model (model 24) for rainy days (black dots) and non-rainy days (black crosses)